DEFORMATION ANALYSIS IN URBAN AREAS USING PERSISTENT SCATTERER

Sang-Wan Kim, Jin Baek, Hyuck Jin Park

Dept. of Geoinformation Engineering, Sejong University
98 Gunja-Dong Gwangjin-Gu, Seoul 143-747, Korea
E-mail: swkim@sejong.ac.kr

ABSTRACT: The permanent scatterer SAR interferometry (PSInSAR) technique has been developed more recently and has been applied to monitor slow but consistent ground subsidence. Since PSInSAR has the advantages in terms of baseline and temporal decorrelation, PSInSAR technique using X-band may also provide useful information about a ground deformation in detail. We developed our codes for a persistent scatterer analysis, and then apply to ERS-1/2 C-band data over Las Vegas in order to validate our new developed algorithm. Based on this test, PS technique using X-band observation such as TerraSAR-X or KOMSAT 5 will be developed.

KEY WORDS: Persistent scatterer, Deformation, PSInSAR, SAR, X-band

1. INTRODUCTION

Many urban areas are experiencing land subsidence due to anthropogenic activities, such as water, oil and natural gas withdrawal (Amelung et al., 1999, Galloway et al., 1999; Hu et al., 2004; Dixon et al., 2006). In addition, some areas also experience subsidence due to natural processes such as sediment compaction (Kim et al., 2005). The novel InSAR technique using the phase at persistent scatterer (or permanent scatterer), PSInSAR, technique has been developed more recently and has been applied to monitor slow but consistent ground subsidence (Ferretti et al., 2000 and 2001). Since PSInSAR has the advantages of having fewer limitations with respect to the baseline and temporal decorrelation, PSInSAR technique using X-band may also provide useful information about a ground deformation in detail.

We developed our codes to apply a persistent scatterer analysis. ERS-1/2 data over Las Vegas were used to test our new developed algorithm. Basically, the test results will show the validation of our algorithm and will compare with X-band observation using TerraSAR-X or KOMSAT 5 in the future. These comparisons would provide useful tests for the general feasibility and accuracy assessment of X-band SAR interferometry technique in urban.

2. DESCRIPTION OF ALGORITHM

A PSInSAR algorithm consists of 3 main procedures:

1. DInSAR processing to generate interferograms after removing the known topographic phase, on a common master using all obtained images.
2. preliminary estimation of DEM error and displacement based on the phase of permanent scatterer candidates
3. final estimation of DEM error and displacement on all pixels using preliminary estimates

The detailed descriptions of PSInSAR algorithm are described by (Colesanti et al., 2003; Ferretti et al., 2001). Here we briefly summarized PSInSAR algorithm to detect surface deformation using multi-temporal SAR image.

The phase of topographically corrected interferogram at location (x) and each time (i) can be described by:

$$\phi_{x,i} = \phi_{defo,x,i} + \phi_{topo,x,i} + \phi_{const,x,i} + \phi_{slope,x,i} + \phi_{atm,x,i} + \phi_{noise,x,i}, \quad (1)$$

where ϕ_{constant}, ϕ_{slope} and ϕ_{atm} (the sum of three components is called APS) are respectively constant phase values, linear phase contributions induced by atmospheric effects and/or orbital fringes, and nonlinear atmospheric effects (Ferretti et al., 2001). The ϕ_{noise} may comprise the temporal decorrelation, spatial decorrelation and thermal noise. The ϕ_{defo} and ϕ_{topo} are phase contribution from ground deformation and DEM error (ε) at each ground target, respectively. From selected potential permanent scatterers (PSs) based on amplitude stability or coherence stability, the APS is estimated by means of exploiting time series of phase value. The estimated APS is interpolated spatially, and then subtracted from each differential interferogram. After removing APS, ground deformation and DEM errors can be computed on a pixel-by-pixel basis in a multi-interferogram framework, based on DEM error is proportional to the only perpendicular component of baseline (distance between satellite orbits) and surface displacement could be a function of time. Two unknown parameters (v and ε) were solved by maximizing the following equation in two-dimensional model space:

$$\Gamma(v,\varepsilon) = \left| \frac{1}{n} \sum_{i=1}^{n} e^{j\cdot(\phi'_{x,i} - \phi_{defo,x,i} - \phi_{topo,x,i})} \right|, \quad (2)$$

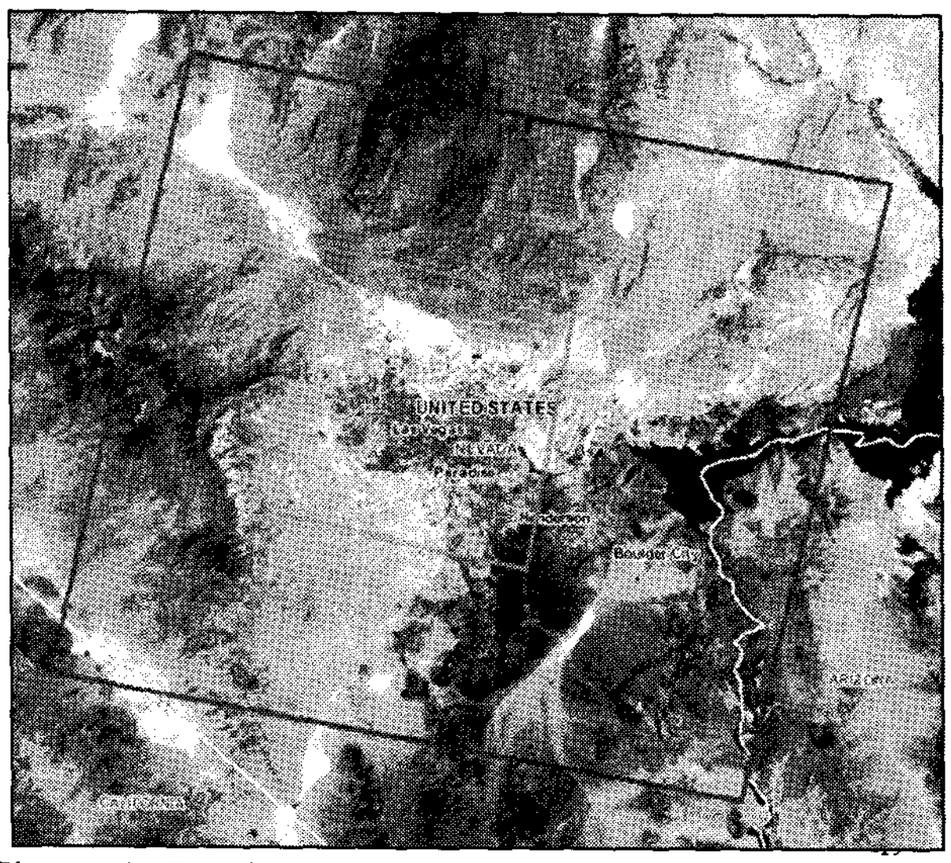

Figure 1. Landsat TM image over the study area, Las Vegas, USA. Outer rectangle represents ERS-1/2 image coverage (about 100 x 100 km) and inner one represents the study area.

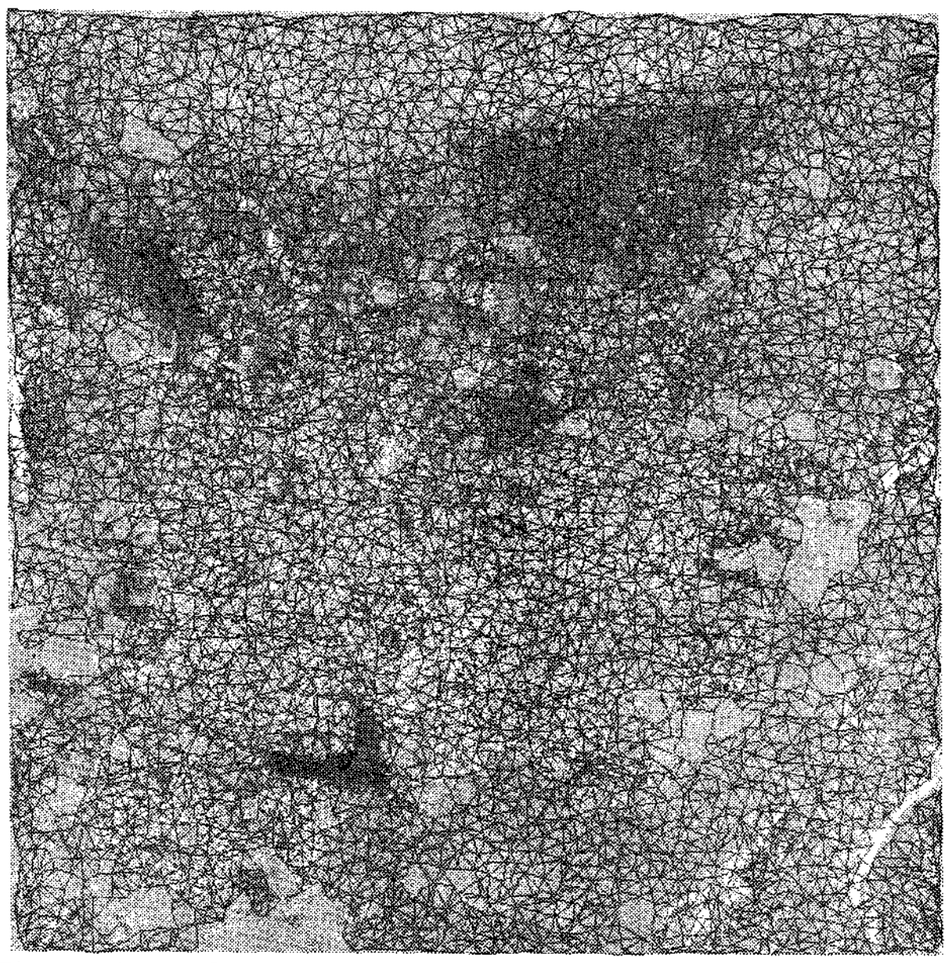

Figure 2. Reference network: approximately 5,100 points were selected as persistent scatterer and 15,000 arcs were generated to get relative estimations between two points in order to reduce an atmospheric effect.

Where n is the number of interferometric pairs and $\phi'_{x,i}$ is a phase in the differential interferogram after removing the APS. Phase coherence Γ ranges from 0 to 1, which can be considered as a reliability measure in fitting a deformation model.

3. DATA PROCESSING

Multi-temporal SAR images are required for applying PSInSAR technique to detect surface deformation. Fifty-three ERS-1/2 C-band SAR data (Track: 356, Frame: 2878) had been acquired over Las Vegas, USA, during April 1992 - September 2000.

We carried out measurements on a subset of image pixels corresponding to point-wise stable reflectors (PS: permanent scatterer). Fifty-two differential interferograms were formed with respect to image acquired on 28 February 1997. Perpendicular baseline and time interval with respect to common master are summarized in Table 1. Delft University of technology was utilized for PSInSAR analysis.

To subtract the topographic contribution from the interferometric phase we used NED 1-arc DEM. We select 5,100 PSCs based on the statistic of backscatter coefficients (Ferretti et al., 2001), subsequently construct a network using TIN as shown in Fig. 2. The maximum length of arc used is 2km. Phase differences of each arc are calculated to estimate displacement parameters and DEM error differences between nearby points so that an atmospheric signal could be reduced at the expense of an additional integration step to get displacement and DEM error at each PSC.

Atmospheric phase in general correlated in spatial domain, but uncorrelated in time while DEM error correlated in perpendicular baseline. In the meantime surface displacement shows the correlation with time, but different degrees of spatial correlation depending on the observed phenomena. Based on the spatial and temporal

Table 1. ERS-1/2 Data set: Bn and Bt denote a perpendicular baseline and acquisition time interval with respect to a master (1997/02/28), respectively.

Sensor	Date	Bn (m)	Bt (day)	Sensor	Date	Bn (m)	Bt (day)
ERS1	19920421	648.93	-1774.0	ERS2	19970124	72.72	-35.0
ERS1	19920526	-515.18	-1739.0	**ERS2**	**19970228**	**0.00**	**0.0**
ERS1	19920908	511.90	-1634.0	ERS2	19970404	337.15	35.0
ERS1	19921117	-436.47	-1564.0	ERS2	19970509	-119.66	70.0
ERS1	19921222	-1012.31	-1529.0	ERS2	19970613	-111.05	105.0
ERS1	19930302	104.55	-1459.0	ERS2	19970718	-112.93	140.0
ERS1	19930406	546.91	-1424.0	ERS2	19970822	276.78	175.0
ERS1	19930824	-593.88	-1284.0	ERS2	19970926	-2.14	210.0
ERS1	19931102	470.89	-1214.0	ERS2	19971031	-930.09	245.0
ERS1	19950330	-759.53	-701.0	ERS2	19971205	121.73	280.0
ERS1	19950817	123.14	-561.0	ERS2	19980109	-154.36	315.0
ERS1	19950921	-237.57	-526.0	ERS2	19980213	-225.40	350.0
ERS1	19951026	815.36	-491.0	ERS2	19980320	60.89	385.0
ERS2	19951027	873.01	-490.0	ERS2	19980424	184.15	420.0
ERS1	19951130	-226.38	-456.0	ERS2	19980529	-59.05	455.0
ERS2	19951201	-255.02	-455.0	ERS2	19990129	-37.60	700.0
ERS1	19960104	205.09	-421.0	ERS2	19990618	-305.09	840.0
ERS1	19960208	495.38	-386.0	ERS2	19990723	565.74	875.0
ERS1	19960418	590.79	-316.0	ERS2	19990827	-1193.99	910.0
ERS1	19960523	-72.68	-281.0	ERS2	19991001	381.67	945.0
ERS2	19960524	-177.16	-280.0	ERS2	19991105	-360.66	980.0
ERS2	19960802	55.59	-210.0	ERS2	19991210	-169.27	1015.0
ERS2	19961011	-317.58	-140.0	ERS2	20000218	-444.64	1085.0
ERS2	19961115	1227.31	-105.0	ERS2	20000428	355.72	1155.0
ERS2	19961220	-355.12	-70.0	ERS2	20000811	544.29	1260.0
				ERS2	20000915	23.28	1295.0

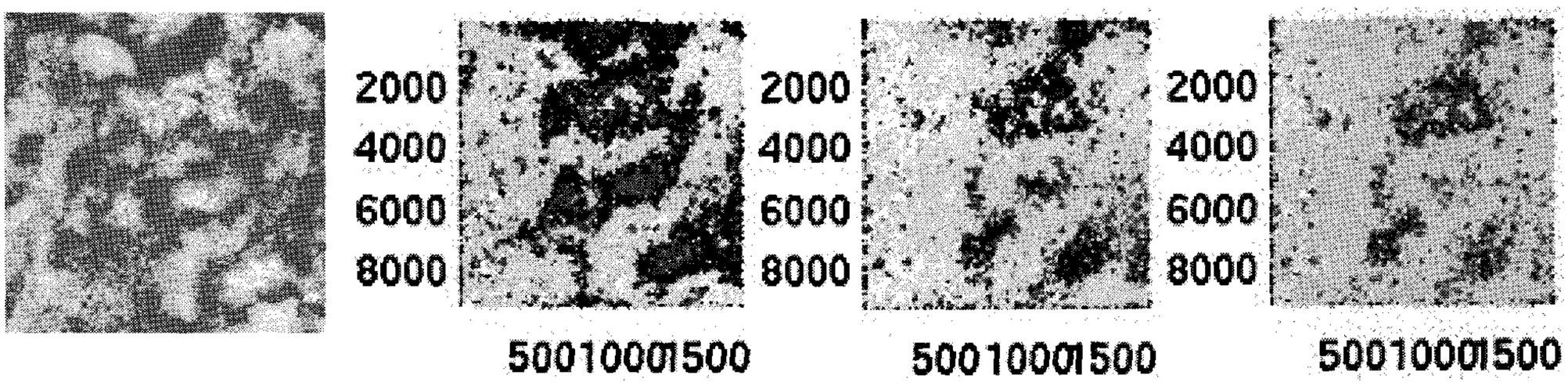

Figure 3. Example of evolution of atmospheric correction: (a) differential interferograms formed from 1997/02/28 and 1998/05/29, (b) scatter plot of phase values at persistent scatterers, (c) and (d) phase values after removing estimated atmospheric phase by first and second iteration, respectively.

characteristic of each component atmospheric phase can be filtered out. Fig. 3, for instance, shows the evolution of atmospheric correction of the differential interferograms (1997/2/28-1998/5/29) by means of iteration processing in our algorithm.

4. OBSERERVED DISPLACEMENT

At this time LOS (Line-Of-Sight) displacement has been converted into vertical displacement on the assumption of pure vertical movements. The vertical mean displacement estimated by PSInSAR technique is shown in Fig. 4. The results indicate continuous and significant subsidence in three sites (white circle in Fig. 4) with about 10 mm/yr velocity and uplift in three sites (black circle in Fig. 4). The subsidence velocity reaches over 15-20 mm/yr in the northern area as the most subsiding block. For more precise analysis, however, we also consider a presumable horizontal movement of surface. In fact surface crack, which could introduce horizontal displacement, induced by lowering groundwater level was reported in this area. Therefore data set observed at more than two different look angle are necessary to separate LOS displacement into vertical and horizontal component. RADARSAT-1 SAR data set at various look angles have been archived over the study

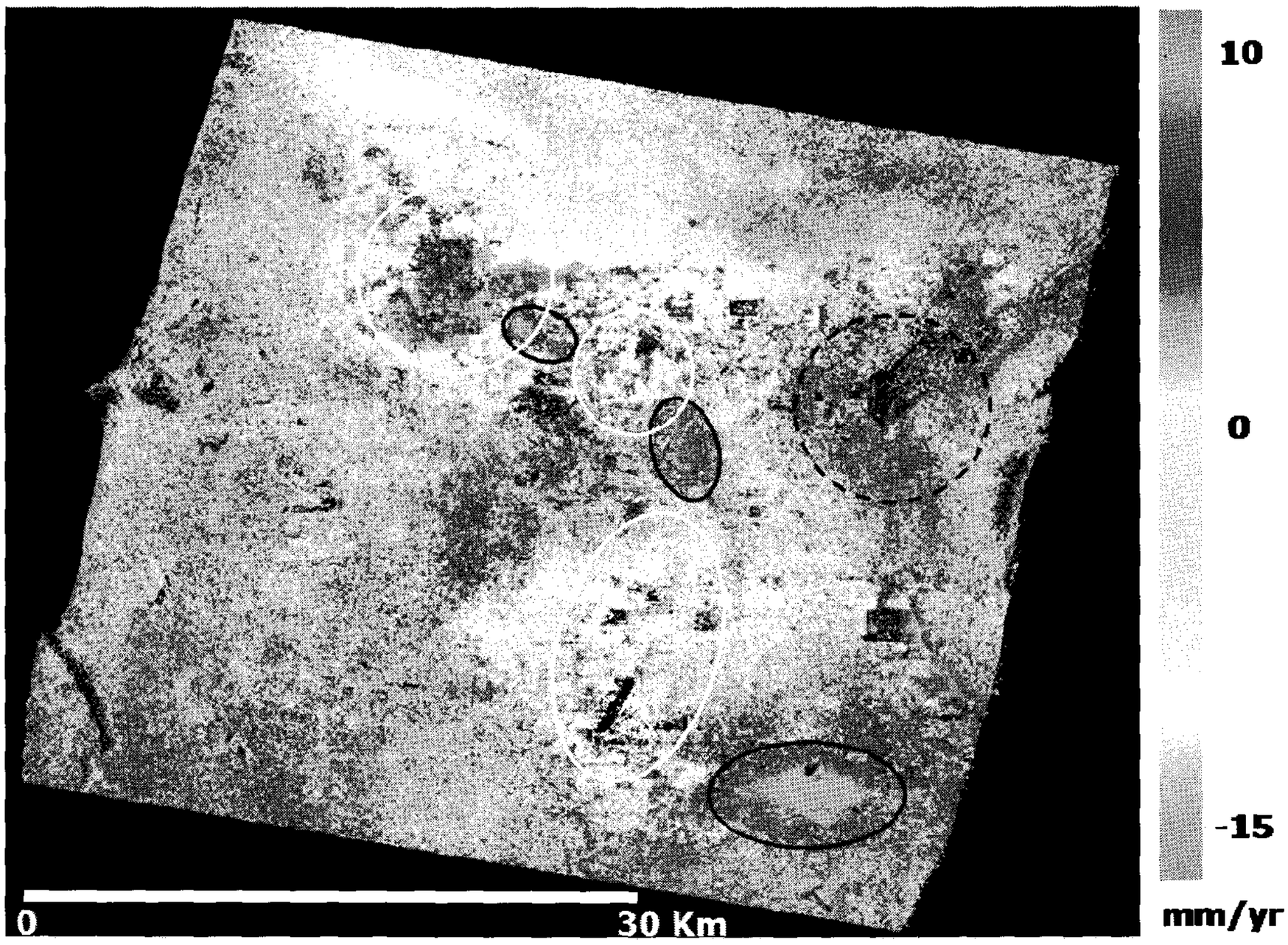

Figure 4. Geo-referenced vertical mean deformation: Background image is the mean reflectivity map. White and black circles represent the block suffering surface deformation of subsidence and uplift, repectively.

area at present. These data sets allow us to measure a displacement along three different directions.

Acknowledgements

The research was supported by the National Research Lab. Project (M1-0302-00-0063) of Korea Ministry of Science and Technology. We also thank KARI (Korea Aerospace Research Institute) for support.

REFERENCES

Amelung F., Galloway D L., Bell J W., Zebker H A. & Laczniak R J., 1999. Sensing the ups and downs of Las Vegas: InSAR reveals structural control of land subsidence and aquifer-system deformation. *Geology*, v. 27, pp. 483-486.

Colesanti, C., Ferretti, A., Novali, F., Prati, C., & Rocca, F., 2003. SAR monitoring of progressive and seasonal ground deformation using the permanent scatterers technique. *IEEE Trans. Geosci. Remote Sens.*, 41, pp. 1685-1701.

Dixon, T.H., Amelung, F., Ferretti, A., Novali, F., Rocca, F., Dokka, R., Sella, G., Kim, S.W., Wdowinski, S., & Whitman, D., 2006. Subsidence and flooding in New Orleans. *Nature*, 441, pp. 587-588.

Ferretti, A., Prati, C., and Rocca, F., 2000. Nonlinear Subsidence Rate Estimation Using Permanent Scatterers in Differential SAR Interferometry. *IEEE Trans. Geosci. Remote Sens.*, 38, pp. 2202-2212.

Ferretti, A., Prati, C., & Rocca, F., 2001. Permanent scatterers in SAR interferometry. IEEE Trans. *Geosci. Remote Sens.*, 39, pp. 8-20.

Galloway, D.L., Jones, D.R., & Ingebritsen, S.E., 1999. Land subsidence in the United States. In. Denver: USGS

Kim, S.W., Lee, C.W., Song, K.Y., Min, K.D., and & Won, J.S., 2005. Application of L-band differential SAR interferometry to subsidence rate estimation in reclaimed coastal land. *International Journal of Remote Sensing, 26*, pp. 1363-1381.

Strozzi, T., Wegmuller, U., Werner, C.L., Wiesmann, A., & Spreckels, V., 2003. JERS SAR interferometry for land subsidence monitoring. *IEEE Trans. Geosci. Remote Sens.*, 41, pp. 1702-1708.